

A Backward-Wave Surface Mode in a Plasma Waveguide

R. N. Carlile

Citation: *Journal of Applied Physics* **35**, 1384 (1964); doi: 10.1063/1.1713638

View online: <http://dx.doi.org/10.1063/1.1713638>

View Table of Contents: <http://scitation.aip.org/content/aip/journal/jap/35/5?ver=pdfcov>

Published by the [AIP Publishing](#)

Articles you may be interested in

[Dual-cavity mode converter for a fundamental mode output in an over-moded relativistic backward-wave oscillator](#)

Appl. Phys. Lett. **106**, 113505 (2015); 10.1063/1.4915892

[Harmonic mode competition in a terahertz gyrotron backward-wave oscillator](#)

Phys. Plasmas **19**, 103103 (2012); 10.1063/1.4757215

[Selective mode suppression in a W-band second harmonic coaxial-waveguide gyrotron backward-wave oscillator](#)

Appl. Phys. Lett. **101**, 033504 (2012); 10.1063/1.4737398

[Dynamics of Mode Competition in the Gyrotron Backward-Wave Oscillator](#)

AIP Conf. Proc. **807**, 191 (2006); 10.1063/1.2158774

[Mode interaction in backward-wave oscillators with strong end reflections](#)

Phys. Plasmas **7**, 1294 (2000); 10.1063/1.873940


**SHIMADZU**
Excellence in Science

Powerful, Multi-functional UV-Vis-NIR and FTIR Spectrophotometers

Providing the utmost in sensitivity, accuracy and resolution for applications in materials characterization and nano research

- Photovoltaics
- Polymers
- Thin films
- Paints
- Ceramics
- DNA film structures
- Coatings
- Packaging materials

[Click here to learn more](#)

Four different models of Shimadzu spectrophotometers are shown. From left to right: a small desktop unit, a larger desktop unit with a sample holder, a large floor-standing unit with a control panel, and a tall, narrow floor-standing unit.

A Backward-Wave Surface Mode in a Plasma Waveguide*

R. N. CARLILE

Department of Electrical Engineering, University of Arizona, Tucson, Arizona

(Received 5 September 1963)

The phase characteristics of a backward-wave pass-band mode have been measured in a plasma waveguide, consisting of a circular waveguide that is coaxial with the positive column of a mercury-vapor discharge. The mode has been identified as an $n=1$ surface mode similar to that described by Trivelpiece.

It is shown that zero-temperature plasma-waveguide theory predicts this mode accurately. This theory predicts that a simple relation exists between the lower cutoff frequency of the $n=1$ mode and the electron plasma frequency. It is demonstrated that the calculated electron plasma frequency obtained from this relation, where the cutoff frequency is determined from a measurement of the phase characteristics, agrees well with an independent measurement of electron plasma frequency by the well-known cavity-perturbation method.

Both the $n=1$ and symmetric $n=0$ modes were excited by a novel coupler called the *double-ring coupler*.

Noise measurements on the $n=1$ and symmetric $n=0$ modes indicate that the output signal-to-noise ratio is independent of input signal power and is about 7 dB for the $n=1$ mode and varies from about 7 to greater than 30 dB for the $n=0$ mode. A simple model of the plasma is proposed which explains all the noise observations reported here. Crawford and Lawson independently proposed a similar model.

I. INTRODUCTION

A PLASMA waveguide is any longitudinally uniform transmission system which has as one of its constituents a plasma. From a structural point of view, one of the simplest plasma waveguides is shown in the inset in Fig. 1. In that inset, the annulus of radii b and a is a glass tube whose function in the experiments to be reported here is to contain the plasma. The surface of radius c is metallic and has a high conductivity.

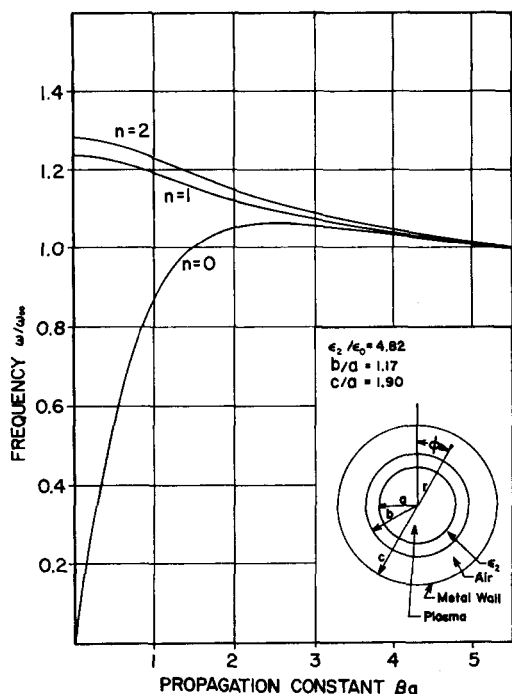


FIG. 1. Phase characteristics for the $n=0, 1, 2$ modes which propagate in the longitudinally uniform plasma waveguide whose cross section is shown in the inset. In the inset, the positive z axis extends into the page.

* Work performed in the Department of Electrical Engineering at the University of California, Berkeley, California.

In 1958, an analysis of this plasma waveguide was made by Trivelpiece¹ in which a quasistatic analysis was used throughout and the resulting modes were slow modes and transverse magnetic (TM). This work was extended by Bevc and Everhart² who carried the solutions into the fast-wave regime. Other workers have analysed this system from specialized points of view.³⁻⁵

If the plasma is isotropic, an infinite set of space-charge modes may exist.¹ These modes are called *surface modes* because their energy tends to be concentrated at the glass-plasma interface, and because there is no charge accumulation inside the plasma, only on the plasma cylinder surface.

The azimuthally symmetric surface mode has been measured by Trivelpiece¹ and by Riedel and Thelen.⁶ Their experimental work has been extended here to include an investigation of the nonsymmetric mode whose field components vary as $\cos\phi$, where ϕ is the azimuthal coordinate (see Fig. 1). This nonsymmetric mode is shown to be a backward wave.

II. THEORETICAL DISCUSSION

An expression for the permittivity of an isotropic plasma ϵ_1 that is in wide use today is⁷

$$\epsilon_1/\epsilon_0 = 1 - (\omega_p/\omega)^2, \quad (1)$$

¹ A. W. Trivelpiece, California Institute of Technology, Pasadena, California, Tech. Report No. 7, (May 1958); also, A. W. Trivelpiece and R. W. Gould, J. Appl. Phys. **30**, 1784 (1959).

² V. Bevc and T. E. Everhart, University of California, Berkeley, California, Inst. Engineering Res. Tech. Report Series No. 60, Issue No. 362, (11 July 1961).

³ P. Rosen, J. Appl. Phys. **20**, 868 (1949).

⁴ T. W. Johnson, RCA Victor, Montreal, Canada, Res. Report, Project No. 4335, (October 1962).

⁵ P. Chorney, Massachusetts Institute of Technology, Cambridge, Massachusetts, Tech. Report No. 277, (26 May 1958).

⁶ H. Riedel and J. Thelen, Electrophysikalisches Institut der Technischen Hochschule, München, Germany, Technical Final Report (1 April 1959 to 31 March 1960).

⁷ S. J. Buchsbaum, L. Mower, and S. C. Brown, Phys. Fluids **3**, 1 (1960).

where ω is the excitation angular frequency, ω_p is the electron plasma angular frequency, and ϵ_0 is the permittivity of free space. This expression for ϵ_1 is valid only if the electrons of the plasma are "cool," collisions can be neglected, and the electron number density is independent of the spatial coordinates.

The quasistatic analysis of the three-region system (air, glass, plasma) shown in the inset of Fig. 1 is given by Trivelpiece,¹ although he does not find all the solutions that we shall need. Trivelpiece shows that an infinite number of modes may exist. All field components of the n th mode have an azimuthal dependence of $\cos n\phi$, and the axial component of the rf electric field

$$\epsilon_0 \left[1 - \left(\frac{\omega_p}{\omega} \right)^2 \right] \frac{I_n'(\beta a)}{I_n(\beta a)} = \epsilon_2 \frac{\epsilon_2 [I_n'(\beta a) K_n'(\beta b) - I_n'(\beta b) K_n'(\beta a)] + \epsilon_0 Q [I_n(\beta b) K_n'(\beta a) - I_n'(\beta a) K_n(\beta b)]}{\epsilon_2 [I_n(\beta a) K_n'(\beta b) - I_n'(\beta b) K_n(\beta a)] + \epsilon_0 Q [I_n(\beta b) K_n(\beta a) - I_n(\beta a) K_n(\beta b)]}, \quad (2)$$

where

$$Q = \frac{I_n(\beta c) K_n'(\beta b) - I_n'(\beta b) K_n(\beta c)}{I_n(\beta c) K_n(\beta b) - I_n(\beta b) K_n(\beta c)},$$

and ϵ_2 is the permittivity of the glass.

In Fig. 1, βa has been plotted versus ω/ω_{co} for $n=0, 1, 2$, where

$$\omega_{co} = \omega_p / (1 + \epsilon_2/\epsilon_0)^{1/2}. \quad (3)$$

The ratios b/a and c/a are those of the experimental plasma waveguide and $\epsilon_2/\epsilon_0 = 4.82$ is the relative permittivity of Pyrex.⁸ It is seen that the symmetric mode ($n=0$) is a low-pass mode. The higher-order modes, however, are backward waves, each occupying a narrow pass band. All modes approach the common cutoff angular frequency ω_{co} at large values of β .

If we consider a two-region system in which the plasma column of radius a is bounded by a material of permittivity ϵ_2 which fills the space between the plasma and the metal wall of radius b , then it can be shown¹ that in the slow-wave regime, the $n=1$ mode is a forward mode again occupying a narrow pass band. As β approaches infinity, ω again approaches the cutoff angular frequency ω_{co} given by Eq. (3). As β becomes very small, though large enough so that we are in the slow-wave regime, ω is given approximately by

$$\omega \approx \omega_u = \omega_p / (1 + P \epsilon_2/\epsilon_0)^{1/2}, \quad (4)$$

where

$$P = \frac{b^2 + a^2}{b^2 - a^2} > 1.$$

We can now discern that in the three-region system the glass tube causes the $n=1$ mode to be a backward wave. At small β , the angular frequency ω_u is determined by the effective permittivity ϵ_2' that is an average of the permittivity of the glass tube and air space

E_z has a radial dependence inside the plasma of $I_n(\beta r)$, where I_n is the n th order modified Bessel function and β is the propagation constant of the n th mode. r and z are the radial and axial coordinates, respectively (see Fig. 1). We assume all field components have an axial dependence of $e^{-i\beta z}$.

In the plasma, E_z and energy of a mode tend to be concentrated at the glass-plasma interface, the concentration increasing for increasing β . In the air space, E_z is a maximum at the air-glass interface and declines to zero at the metal wall. For the three-region system, the determinantal equation for β is¹

weighted approximately according to the volume occupied by each, because for β very small, a large portion of the energy in the electric field will be found in the air space.

As β increases, the energy in the electric field becomes increasingly concentrated in the glass tube. Thus, the effective permittivity of the glass and the air space approaches that of the glass so that ω_{co} is continually decreasing. In the limit of infinite β the effective permittivity is just that of the glass ϵ_2 which can cause ω_{co} to be less than ω_u with the result that the $n=1$ mode will be a backward wave.

III. APPARATUS

A longitudinal cross section of the plasma waveguide used in the experiments is shown in Fig. 2. The plasma was the positive column of a mercury-vapor discharge which employed a hot cathode. The pressure of the mercury vapor was approximately 2×10^{-3} Torr.

Traveling surface modes were excited by a *double-ring coupler*, described below, and were absorbed by a tapered Aquadag termination. The traveling-wave fields were probed in the air region by a small probe which could move longitudinally and which coupled to

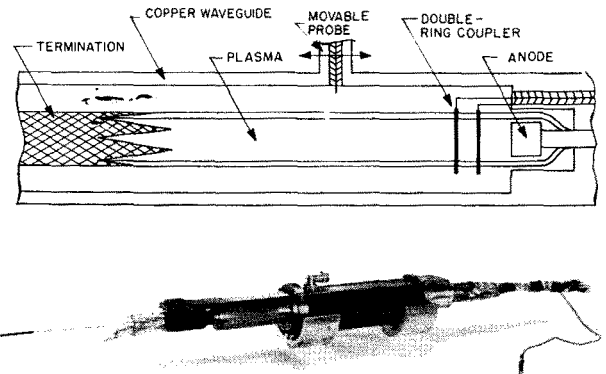


FIG. 2. The experimental plasma waveguide: drawing of longitudinal cross section and photograph of the assembled system.

⁸ *Dielectric Materials and Applications*, edited by A. R. von Hippel (Tech. Press, Cambridge, Massachusetts, and John Wiley and Sons, Inc., New York, 1954).

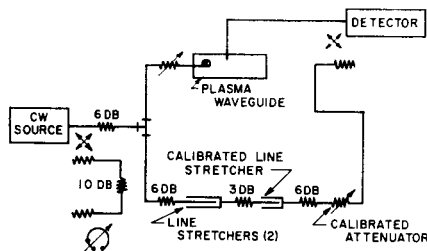


FIG. 3. Microwave bridge circuit.

the radial electric field component E_r of the mode. The microwave bridge circuit shown schematically in Fig. 3 made it possible to continuously monitor the phase of a propagating wave as a function of distance.

The double-ring coupler is shown in Figs. 2 and 4. It consists of two metal rings which fit tightly over the glass tube and whose planes are parallel to one another. The rings are connected to the inner and outer conductors, respectively, of a coaxial transmission line.

In Fig. 5, the voltage standing-wave ratio (VSWR), looking into the coaxial transmission line driving the coupler, is shown as a function of frequency. Also shown in this figure are the corresponding propagation constants (β) of the $n=0$ and $n=1$ surface modes that were excited by the coupler. It is seen that when β is large, the VSWR is small, reaching a minimum of 1.4. The smallness of the VSWR may be understood by recalling that as β increases, the energy in the $n=0$ and $n=1$ modes becomes increasingly concentrated in the region of the coupler, which is the condition one would expect for maximum coupling. For smaller values of β , the energy is less concentrated in the region of the coupler so that the coupler is less effective in coupling energy into the modes.

This coupler, which employs geometrically symmetric rings, was able to excite the nonsymmetric $n=1$ mode, probably, because the electric field between the rings is nonsymmetric. The electric field is probably greatest at the point at which the rings are fed from the coaxial transmission line and declines to a minimum on the opposite side of the rings. No measurements have been made to determine the maximum and minimum values of the field. If $\phi=0$ occurs at the point at which the rings are fed, according to the above reasoning, the

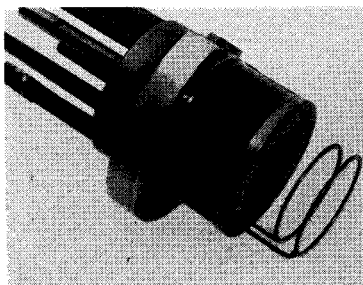


FIG. 4. The double-ring coupler.

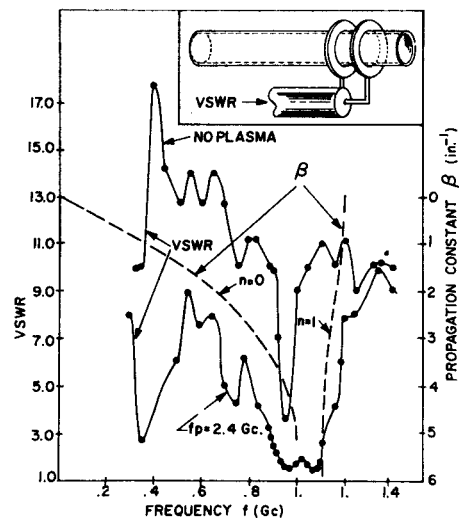


FIG. 5. Voltage standing-wave ratio (VSWR) of the double-ring coupler.

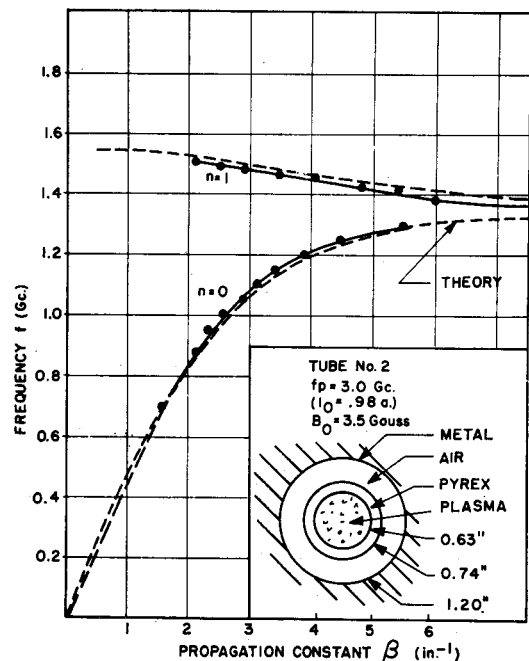
electric field between the rings would vary as

$$1 + A \cos \phi, \quad A < 1.$$

The first term, unity, will cause the $n=0$ mode to be excited, whereas the second term, $A \cos \phi$, will cause the $n=1$ mode to be excited.

IV. PROPAGATION CONSTANT MEASUREMENTS

Plots of ω vs β for the $n=1$ and the accompanying $n=0$ modes are shown in Figs. 6-8. The magnetic

FIG. 6. Phase characteristics for $n=0, 1$ modes for $f_p = 3.0$ Gc/sec. Error in β : approximately $\pm 3\%$.

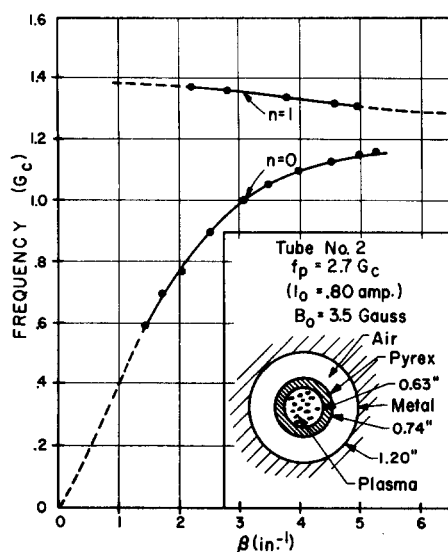


FIG. 7. Phase characteristics for $n=0, 1$ modes for $f_p = 2.7$ Gc/sec. Error in β : approximately $\pm 3\%$.

field in these measurements, and in all measurements reported here, was 3.5 G. High attenuation limited the range over which the propagation constant β could be measured.

We have confirmed experimentally that the field components of the $n=0$ mode are independent of ϕ , while the $n=1$ field components have a $\cos\phi$ variation. This was done by holding the detection probe fixed and rotating both the coupler and discharge tube as a unit. Radial plots of a quantity proportional to E_r vs ϕ are shown in Figs. 9 and 10 for the $n=1$ and $n=0$ modes, respectively. Although both plots differ from the mathematically ideal (dashed curves), it is clear that a $\cos\phi$ dependence is predominant in Fig. 9 while Fig. 10 shows that the $n=0$ mode is independent of ϕ . The distortion of these plots probably is due to the glass wall not being of uniform thickness. In a similar glass tube, the wall thickness varied by about 4%.

In the measurements that have been discussed above, the backward-wave nature of the $n=1$ mode was

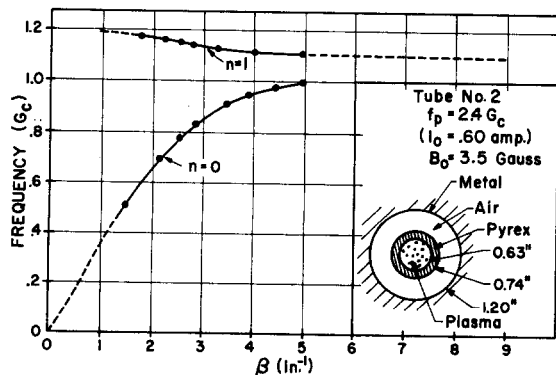


FIG. 8. Phase characteristics for $n=0, 1$ modes for $f_p = 2.4$ Gc/sec. Error in β : approximately $\pm 3\%$.

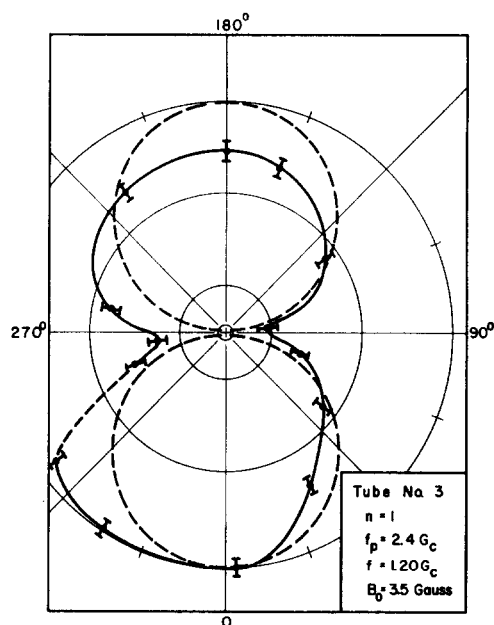


FIG. 9. $n=1$ mode. Radial plot of a quantity proportional to E_r vs the azimuthal coordinate ϕ (solid curve). Dashed curve is proportional to $|\cos\phi|$.

extremely evident. Call βz the phase of a mode at $z=0$ is the position of the coupler. Continuous monitoring of the phase of a mode was possible by balancing a change in phase shift through the plasma waveguide with an equal change in phase shift through the calibrated line stretcher shown in Fig. 3. For the $n=0$ mode, as the detection probe was moved away from the coupler, the line stretcher had to be extended in order to keep the bridge in balance, thus indicating a

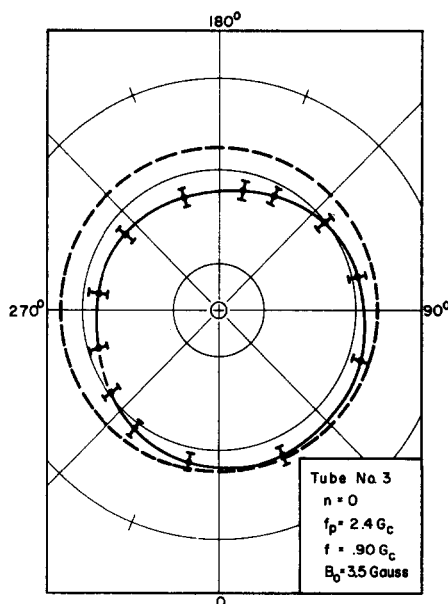


FIG. 10. $n=0$ mode. Radial plot of a quantity proportional to E_r vs the azimuthal coordinate ϕ (solid curve). Dashed curve is a reference circle.

wave whose phase was *lagging* with increasing z . This type of phase variation is characteristic of a forward wave.

At a frequency in the $n=1$ pass band, as the detection probe was moved *away* from the coupler, the line stretcher had to be shortened, thus indicating a wave whose phase *advanced* with increasing z . This type of phase variation is characteristic of a backward wave where the phase velocity is toward the coupler while the energy velocity must be away from the coupler (the energy velocity must be away from the coupler for any wave.)

Attenuation measurements have been made on both the $n=1$ and $n=0$ modes although the results are not shown. In general, they confirm qualitatively the theoretical relationship⁹ between the attenuation constant α and the group velocity $d\omega/d\beta$,

$$\alpha = \frac{1}{2}\nu / (d\omega/d\beta), \quad (5)$$

where ν is the electron collision frequency, assumed to be a constant. Equation (5) will predict an electron collision frequency of the order of 100 Mc/sec where α and $d\omega/d\beta$ have been obtained from the experimental data.

We would now like to determine how well the theory developed in Sec. II above predicts the experimental results, in particular, the curves for the $n=0$ and $n=1$ modes shown in Fig. 6.

The theoretical results presented in Fig. 1 have been obtained for the dimensions of the experimental plasma waveguide. Thus, these results may be directly compared with the experimental results of Fig. 6 if the parameter $f_{co} = \omega_{co}/2\pi$, the cutoff frequency, is available. f_{co} cannot be determined directly from Fig. 6 because it was not possible (due to high attenuation) to make measurements at large enough values of β to determine to what frequency the two curves are becoming asymptotic. Therefore, the following procedure was adopted: f_{co} was chosen so that a theoretical curve would coincide exactly with the corresponding experimental curve at $\beta = 4.50$ (in.)⁻¹.

From Fig. 1, at $\beta = 4.50$ (in.)⁻¹ ($\beta a = 1.42$), $f/f_{co} = 0.99$ for the $n=0$ mode and $f/f_{co} = 1.16$ for the $n=1$ mode. Now referring to Fig. 6 at $\beta = 4.50$ (in.)⁻¹, $f = 1.24$ Gc/sec for the $n=0$ mode and $f = 1.44$ Gc/sec for the $n=1$ mode. Thus, the theoretical $n=0$ mode will coincide with the experimental $n=0$ curve at $\beta = 4.50$ (in.)⁻¹ if $f_{co} = 1.25$ Gc/sec while the theoretical and experimental $n=1$ curves will coincide at $\beta = 4.50$ (in.)⁻¹ if $f_{co} = 1.24$ Gc/sec. Arbitrarily, let

$$f_{co} = 1.24 \text{ Gc/sec.}$$

The resulting theoretical curves for the $n=0$ and $n=1$ modes are shown as dashed curves in Fig. 6. We

note the close agreement nearly everywhere between theory and experiment. In fact, we confirm that the value of β chosen to make a theoretical and experimental curve coincide for the purpose of determining f_{co} is entirely arbitrary. Any value of β could have been chosen yielding nearly the same f_{co} , so that the same excellent agreement between theory and experiment would have been obtained.

From Eq. (3), we note that there is a definite relationship between f_{co} and the plasma frequency $f_p = \omega_p/2\pi$. For $f_{co} = 1.24$ Gc/sec, the corresponding plasma frequency is $f_p = 3.0$ Gc/sec, where we have taken $\epsilon_2/\epsilon_0 = 4.82$, the permittivity of Pyrex.

We now wish to obtain an independent check on this value of the plasma frequency. This may be done most easily by using the well-known cavity-perturbation technique in which the discharge tube and a cylindrical cavity are located coaxially with respect to each other.⁷ The cavity is then excited in its TM₀₁₀ mode, and we observe the difference in resonant frequencies of this mode for the conditions of plasma on and plasma off. For a proper choice of the dimensions of the system and if f_p/f_0 is not too large,⁹ where f_0 is the resonant frequency of the cavity with the plasma on, then f_p^2 will be proportional to the shift in resonant frequencies with small error.

In Fig. 6, the discharge current is 0.98 A. For the same discharge current, the cavity perturbation measurement indicates that $f_p = 3.2$ Gc/sec, which is about 7% higher than the value 3.0 quoted above which was obtained from the phase characteristics of Fig. 6.

It is of considerable interest to make a large number of comparisons of f_p determined from Eq. (3) with f_p determined by the cavity-perturbation technique. From the data that were taken, it has been possible to make nine comparisons.

These nine comparisons showed that the values of f_p found in these two different ways differed on the average by 6.2%. The largest deviation was 11% and the smallest 2%. In all cases the cavity-determined f_p was larger than the f_p found from Eq. (3).

V. NOISE MEASUREMENT

For a mode propagating in the plasma waveguide, the total power that flows across a cross section of the system may be represented as the sum of two terms,

$$P = P_s + P_N,$$

where P_s is the power at the transmitter or signal frequency f and P_N is the unwanted power at all other frequencies which we call the *noise power*. In this section, we shall describe measurements that have been made on the signal-to-noise ratio, $10 \log (P_s/P_N)$, for the $n=0$ and $n=1$ modes.

We have found experimentally that the noise output of the transmitter (signal source) is very small compared to P_N so that P_N is nearly all generated in the

⁹ R. N. Carlile, Doctoral dissertation, University of California (1963); also, University of California Electronics Res. Lab. Tech. Memo. TM-30 (12 August 1963).

plasma waveguide. If we probe a mode with the detection probe, we shall assume that the signal power and the noise power absorbed by the probe and which travel down the coaxial transmission line to the measuring apparatus will have the same ratio as P_S and P_N at the position of the probe.

The method of measurement of $10 \log (P_S/P_N)$ made use of the microwave bridge circuit shown in Fig. 3 where the null detector was a high-sensitivity receiver capable of accurate measurement of relative power levels. Disconnecting the reference arm of the bridge which contains the line stretcher and attenuator, the power level of the signal arriving from the detection probe is noted. This power is proportional to the total power P . We now connect the reference arm of the bridge and balance out the transmitter frequency component of the signal. Thus, the only power which can now reach the receiver is proportional to P_N so that we are able to measure $10 \log (P/P_N)$. From this, $10 \log (P_S/P_N)$ is easily obtained.

Measurements of this type have been made on both the $n=0$ and $n=1$ modes. We find that $10 \log (P_S/P_N)$ is independent of the input power level to the plasma waveguide. Here, the input power was varied from about 1 to 0.1 mW.

In Fig. 11 we show the variation of $10 \log (P_S/P_N)$ as a function of frequency for the detection probe far from the double-ring coupler. The noise power *increases* relative to the signal power for the $n=0$ mode as f_{co} is approached. For the $n=1$ mode, $10 \log (P_S/P_N)$ is nearly constant across its band. In Fig. 12, $10 \log (P_S/P_N)$ is shown as a function of the probe position at discrete frequencies. In all cases, the noise power *decreases* relative to the signal power as the input coupler is approached.

We have examined the signal emerging from the detection probe with a spectrum analyzer which had a 1000-cps sweep rate, i.e., the spectrum analyzer will display the spectrum of the signal on the cathode-ray tube screen at millisecond intervals. From observations

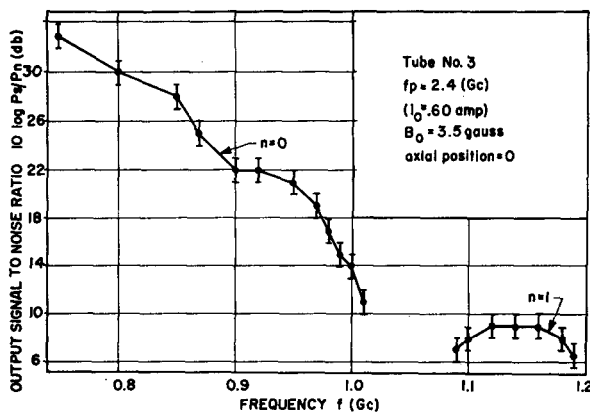


FIG. 11. Signal-to-noise ratio for $n=0, 1$ modes vs frequency at an axial position near the termination. $f_p = 2.4$ Gc/sec.

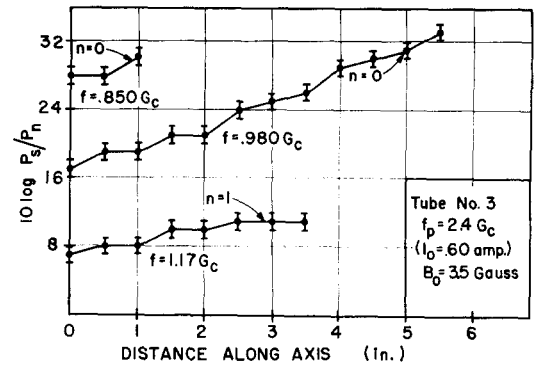


FIG. 12. Signal-to-noise ratio for $n=0, 1$ modes vs axial position. The positions indicated by 0 and 6 in. are near the termination and coupler, respectively.

on the spectrum analyzer, it was possible to determine that if E_{r1} is the radial field component which excites the detection probe at time t_1 , then a millisecond later at t_2 , the radial field component E_{r2} will be slightly different in either amplitude, phase, or both, from E_{r1} . A millisecond later, at t_3 , E_{r3} will be slightly different from E_{r2} , etc. Thus, there appears to be a small amplitude modulation, phase modulation, or both, of the signal frequency at the position of the detection probe, and P_N is therefore the power in the sidebands which exists by virtue of this modulation. It was also possible to determine from observations on the spectrum analyzer that the modulation frequencies were less than 1 Mc/sec.

We now propose a simple model of the plasma which will explain all the experimental information presented above. Assume that the electron number density n_e consists of a part which is independent of time n_{e0} and a small time-varying part $\Delta n_e(t)$, so that,

$$n_e = n_{e0} + \Delta n_e(t). \quad (6)$$

n_{e0} may be regarded as a time average of n_e while $\Delta n_e(t)$ is a noise fluctuation of n_e whose frequency components are less than 1 Mc/sec. Assume that $\Delta n_e(t)$ is independent of position so that the electron density everywhere in the positive column is fluctuating coherently.

Equation (6) for n_e will lead to a plasma angular frequency

$$\omega_p = \omega_{p0} + \Delta \omega_p(t), \quad (7)$$

and a cutoff angular frequency

$$\omega_{co} = (\omega_{co})_0 + \Delta \omega_{co}(t). \quad (8)$$

If the $n=0$ or the $n=1$ mode is propagating in the system with a propagation constant β and an attenuation constant α , then,

$$\beta = \beta_0 + \Delta \beta(t), \quad (9)$$

and

$$\alpha = \alpha_0 + \Delta \alpha(t). \quad (10)$$

In the above expressions, a quantity with a subscript "0" is a time-average quantity while a quantity preceded by Δ is a noise fluctuation of the quantity due to $\Delta n_e(t)$.

If the probe is a distance L from the coupler, then E_r , the component of the electric field to which the detection probe is sensitive, will be related to E_r at the coupler by the factor

$$\exp(-\alpha L - i\beta L) = \exp(-\alpha_0 L - i\beta_0 L) \times \exp[-\Delta\alpha(t)L] \exp[-i\Delta\beta(t)L]. \quad (11)$$

The factors

$$\exp[-\Delta\alpha(t)L] \quad \text{and} \quad \exp[-i\Delta\beta(t)L]$$

will account for the amplitude and phase modulation, respectively, of the wave, and P_N will be the power in the side bands which is due to them.

It is clear now that $10 \log (P_S/P_N)$ will be independent of the input power supplied by the transmitter because the system is *linear*.

To explain qualitatively the variation of $10 \log (P_S/P_N)$ shown in Figs. 11 and 12, consider a particular angular frequency ω_k in the noise frequency spectrum. Suppose the component of $\Delta n_e(t)$ at this frequency is $\Delta n_{ek} \sin \omega_k t$, so that the factors producing amplitude and phase modulation at ω_k in Eq. (11) are

$$\exp[-\Delta\alpha_k L \sin(\omega_k t + \theta')]$$

and

$$\exp[-i\Delta\beta_k L \sin(\omega_k t + \theta'')],$$

respectively. The greater are $\Delta\alpha_k L$ and $\Delta\beta_k L$, the more power there will be in the side bands associated with ω_k . The same is true at all other noise frequencies.

Referring to Figs. 6-8, and Eq. (5), it can be seen that a fluctuation in ω_{co} at the noise angular frequency ω_k of amplitude $\Delta(\omega_{co})_k$ will cause both $\Delta\beta_k$ and $\Delta\alpha_k$ to increase as the transmitter angular frequency approaches $(\omega_{co})_0$. Thus, for constant P_S and L , P_N will increase as the transmitter angular frequency approaches $(\omega_{co})_0$. This dependence of P_N on the transmitter frequency is in agreement with the variation of $10 \log (P_S/P_N)$ shown in Fig. 11. At a constant transmitter frequency, if the detection probe is moved toward the coupler so that L decreases, then $\Delta\alpha_k L$ and $\Delta\beta_k L$ will decrease and therefore P_N will decrease which is in agreement with the variation of $10 \log (P_S/P_N)$ shown in Fig. 12.

The model of the plasma that we have made use of above and which is summarized by Eq. (6) has been predicted approximately by Crawford and Lawson.¹⁰ They find that in a mercury-vapor discharge, except for a region extending about 20 cm in front of the cathode, there is a noise fluctuation of the electron

number density which is coherent from point to point. The diameter of their discharge was 2 cm and they operated at a discharge current of approximately 0.1 A. All measurements reported in this section were made near the anode where presumably the fluctuations of n_e were coherent.

Crawford and Lawson postulate that there is a source of noise power in the region near the cathode and that waves of noise voltage propagate down the positive column with phase velocities greater than 10^9 cm/sec. The spectrum of the noise voltage frequencies shows predominant components at 60 and 105 kc/sec at 0.1 A discharge current. They have measured relative fluctuations in n_e and find that they become somewhat greater as the cathode is approached.

VI. ERROR

Slow drift of the total phase shift of a mode from the double-ring coupler to the detection probe was the chief cause of error in the propagation constant measurements. This drift is probably due to a drift in the vapor pressure of the mercury which causes the parameters of the discharge (such as electron density) to vary. We have been able to estimate that drift in phase shift caused a $\pm 3\%$ error in the measurement of β . The amplitude of a mode at the position of the detection probe was also observed to drift by a few tenths of a dB over a 7-min observation period.

VII. SUMMARY AND CONCLUSIONS

We have examined experimentally the $n=1$ surface mode in a plasma waveguide of circular symmetry. Experimentally and theoretically this mode is a backward wave for the particular plasma waveguide used in the experiments. Using a simple model of the plasma, we have predicted the propagation constant of the $n=1$ mode and also of the $n=0$ mode with considerable precision.

Since the $n=1$ mode is a backward wave, one might expect that its interaction with an electron beam might result in backward-wave oscillation. This possibility is made even more attractive by realizing that the bandwidth and maximum group velocity of the $n=1$ mode may be varied within wide limits by a suitable choice of c/a , b/a , and ϵ_2 . For example, for $c/a=1.9$, $b/a=1.1$, and $\epsilon_2=10$, the upper cutoff frequency of the $n=1$ mode is $1.7f_{co}$.

Unfortunately, the positive column of the mercury-vapor discharge is clearly not a suitable plasma for a practical, backward-wave oscillator, because of three detracting characteristics: drift of the parameters of the discharge, significant noise modulation of the signal, and loss. It is conceivable that the first two could be reduced, but it is doubtful that they could be eliminated. Thus, we must look elsewhere for a suitable plasma medium.

¹⁰ F. W. Crawford, and J. D. Lawson, Plasma Phys.-Accelerators-Thermonucl. Res. 3, 179 (1961).

ACKNOWLEDGMENTS

The author wishes to thank Professor T. E. Everhart and Professor A. W. Trivelpiece of the University of California, and Professor G. S. Kino of Stanford University for helpful discussions. Thanks are also extended to G. Becker who constructed the experimental tubes.

This work was supported in part by the Air Force Office of Scientific Research of the Office of Aerospace Research; the Department of the Army, Army Research Office; and the Department of the Navy, Office of Naval Research, under Grants AF-AFOSR62-340 and AF-AFOSR139-63. Partial support was also provided through a Ford Foundation Fellowship.

JOURNAL OF APPLIED PHYSICS

VOLUME 35, NUMBER 5

MAY 1964

Statistics of Time in Photomultiplication

RAYMOND EULING

Lincoln Road, Sudbury, Massachusetts

(Received 1 October 1962; in final form 9 October 1963)

Photomultiplication is considered as a branching process. The output current of the photomultiplier is studied as a function of the statistical distributions of photon emission, electron flight times, and secondary emission yields. Expressions are derived for the timing accuracy of photomultipliers and scintillation counters.

1. INTRODUCTION

AN event which causes a flash of light can be timed by recording the flash. An essential part of many recording instruments is a photomultiplier tube. Each photon has a possibility of causing a cascade of electrons to appear at the output of the photomultiplier so that, in response to the flash of light, a brief current is generated.

The duration of the current is longer than the time intervals of interest, therefore some function of this current must serve as a time reference mark. If the mean time between the beginning of the flash and the mark is deducted from the time value of the mark, an estimate of the time of the event is obtained. This estimate is subject to statistical error, and it is the purpose of this paper to relate this error to some properties of the flash and of the photomultiplier.

2. PREVIOUS ANALYSES

A rough way of representing the cascade output current $I(t)$ is to assume¹ it is given invariably by the Gaussian function

$$I(t) = \bar{I}(t) = [I_0 / (2\pi)^{1/2} \sigma] e^{-(t-t_m)^2 / 2\sigma^2}.$$

The parameters are found by making a large number of measurements and averaging.

The variance of the mark function

$$T \equiv \bar{t} = \int t I(t) dt / \int I(t) dt,$$

the average time of arrival, has been expressed as a

¹ E. Baldinger and W. Franzen, *Advan. Electron.* **8**, 301 (1956).

function of the variances of independent flight times between pairs of surfaces, assuming the probability density functions (pdf) of flight time are Gaussian and the multiplication at any surface is a constant.² [See Eq. (6).] The half-width of the average output current curve is $D^{1/2}\sigma$, where D is the number of multiplying dynodes and σ is the standard deviation of the flight time between any pair of surfaces.³ The standard deviation of the time at which the first photoelectron due to a scintillation flash leaves the photocathode of the photomultiplier tube has been calculated,⁴ assuming a scintillation crystal described by a single decay constant and a fixed number of photons. The statistics of the time of arrival at the first dynode of the n th photoelectron due to a scintillation flash has been calculated⁵ assuming that the flight time pdfs are exponential in form and that the secondary emission yields are constant.

The pdf of the total number of electrons in a cascade is given in Ref. 6, and springs from the work of S. Ulam, D. Hawkins, and others. A computation⁷ of this pdf for the case of Poissonian pdfs of secondary emission yield has been done numerically. The results were thought not to fit the facts and doubt was expressed about the assumption of the Poisson function. However, later experiments⁸ with single-electron cascades agreed very

² G. A. Morton, Symposium on Millimicrosecond Techniques, University of California, February, 1957.

³ G. A. Morton, *Advan. Electron.* **4**, 87 (1952).

⁴ R. F. Post and L. I. Schiff, *Phys. Rev.* **80**, 1113 (1950).

⁵ M. A. El-Wahab and J. V. Kane, *Nuc. Inst. Meth.* **15**, 15 (1962).

⁶ W. Feller, *Probability Theory and its Applications* (John Wiley & Sons, Inc., New York, 1950), p. 223.

⁷ E. J. Lombard and F. Martin, *Rev. Sci. Instr.* **32**, 200 (1961).

⁸ R. F. Trusting, Q. A. Kerns and H. K. Knudsen, University of California Report UCRL-9980 (1962).